Green-Synthesized Nickel-Doped Strontium Oxide Nanocomposite for Efficient Catalytic Degradation of Naphthol Blue Black Dye

R. Lavanya, B. Vinitha, G. Selvakumar

Department of Chemistry, Jawahar Science College, Neyveli-607803, India.

DOI: https://doi.org/10.51244/IJRSI.2026.1305000101

Received: 04 May 2026; Accepted: 09 May 2026; Published: 01 June 2026

ABSTRACT

Naphthol Blue Black is an organic contaminant that is produced by the wood, textile, and dye industries. Many studies have been undertaken to investigate the cleanup of Naphthol Blue Black from industrial effluents. SrO nanoparticles are now being utilized to remove Naphthol Blue Black colours from water. We used a green synthesis to create strontium oxide nanoparticles for photocatalytic NBB breakdown under light conditions. To enhance the solar light activity and avoid charge recombination, we employed a green synthesis from *albizia amara* leaves extract to add Ni as a dopant in strontium oxide nanoparticles. Strong base NaOH, nickel nitrate, and strontium nitrate were used as precursors. The nanoparticles were crushed into powder and calcined at 450 °C in a muffle furnace to produce SrO and Ni-doped SrO nanoparticles. The nanoparticles were analysed using several analytical methods to determine their morphological and structural properties. At 309, 312, and 317 nm, UV-V is spectroscopy showed absorbance values of SrO doped with nickel. The Ni–O stretching peak was identified in the FTIR analysis of strontium oxide nanoparticles at 402 cm^{-1} and 581 cm^{-1} , whereas the Sr–O bond gave a signal at 854.84 cm^{-1}. SEM images of Ni-doped SrO nanoparticles were created at various magnifications. The nanostrips are hexagonal and cylindrical. Sherrer's equation was used to compute the average crystalline structure, which showed that the diameters of pure and Ni-doped SrO nanoparticles were 44.84 and 42.93 nm. According to the EDX examination, Ni-doped SrO is about 70 % Sr and oxygen, with around 1.34 %Ni. The resulting sample was tested for photocatalytic degradation of Naphthol Blue Black, and the completion of the reaction was monitored using UV-visible spectroscopy to measure the % photocatalytic degradation during light illumination. According to the UV-visible spectra, 90% of the dye was effectively destroyed.

Keywords: Dye degradation, naphthol blue black, photocatalyst, nanocomposite, green synthesis.

INTRODUCTION

Access to safe and clean drinking water is a basic human right, as highlighted by the World Health Organization (WHO), which actively monitors global access to non-toxic water resources. The organization emphasizes that every individual, regardless of age or socio-economic background, should have reliable access to safe drinking water. Therefore, preventing environmental contamination and effectively controlling existing pollutants are of atmost importance.

At the same time, growing energy demands, environmental concerns, and the rapid depletion of fossil fuels have driven the search for sustainable, renewable, and low-cost energy sources. In this context, photocatalytic water splitting and the degradation of pollutants using solar energy have emerged as clean and environmentally friendly methods for hydrogen production.

Recently, multiferroic materials have attracted significant interest due to their ferroelectric properties and narrow band gaps, which enable efficient absorption of visible light. These characteristics make them promising candidates for applications in both photovoltaics and photocatalysis. Moreover, increasing industrialization and population growth have intensified environmental issues, particularly water pollution, underscoring the urgent need for effective and sustainable solutions.

ISSN No. 2321-2705 | DOI: 10.51244/IJRSI |Volume XIII Issue V May 2026

Photocatalysis is increasingly recognized as a cutting-edge and environmentally friendly technology for the degradation of organic contaminants. Its application in wastewater treatment has been extensively studied in recent years. Compared to conventional physical and biological treatment methods, photocatalysis is relatively cost-effective and simpler to operate. However, despite the use of various photocatalysts for degrading naphthol blue black (NBB), their practical applications remain limited due to challenges such as high charge recombination rates, limited visible-light absorption, unclear degradation mechanisms, and weak surface catalytic activity.

Recent advances in nanotechnology have enabled the development of economically viable and environmentally stable systems for effective wastewater treatment, meeting the ever-growing demand for improved water quality. Numerous techniques—such as coagulation, adsorption, calcination, filtration, and advanced oxidation processes—have been employed to remove hazardous contaminants from industrial wastewater. Although these methods can be effective, they are not universally applicable, as each technique targets specific types of pollutants. Moreover, many of these approaches involve high operational costs and may generate secondary pollutants, some of which can be more harmful than the original contaminants. Therefore, there is a critical need to develop more efficient and sustainable treatment strategies.

Nanomaterials have emerged as one of the most advanced solutions in wastewater treatment due to their high surface-to-volume ratio, which enhances their interaction with pollutants. In aqueous systems, nanoparticles can exhibit unique behaviors such as colloidal stability and quantum size effects, contributing to improved adsorption, interfacial interaction, and reaction efficiency. Additionally, their small size enables energy and cost savings.

Among various treatment approaches, advanced oxidation processes (AOPs) and photocatalysis have gained significant attention due to their high efficiency in degrading and mineralizing organic pollutants. Photocatalysis, in particular, is considered more environmentally benign than conventional physical and chemical methods, as it does not produce harmful residues or simply transfer pollutants from one phase to another.

Naphthol blue black (NBB) has been selected as the target pollutant due to its high environmental toxicity. It is an azo dye containing phenolic, anilino, naphthalene, and sulfonated groups, which contribute to its stability and resistance to degradation. NBB is widely used in the textile industry for dyeing materials such as wool, nylon, and silk, as well as in textile printing. Additionally, it is used in applications such as soap coloring, anodized aluminum finishing, casein coloring, wood staining, and ink production. Its high photochemical and thermal stability, along with its widespread industrial use, makes it a significant environmental concern and an important subject for degradation studies.

MATERIAL AND METHODS

Preparation of Ni-doped SrO

Albizia amara plants have a wide range of biomolecules and metabolites, including vitamins, proteins, coenzyme-based intermediates, flavonoids, phenols, and carbohydrates.[24-25] Carbonyl, hydroxyl, and amino functional groups in such plant compounds interact with metal ions to reduce their particle size to the nanoscale. Flavonoids include a variety of functional groups, but the–OH group is thought to be the most important for changing metal ions to NPs. These compounds also play a critical role in the capping of nanoparticles, which is critical for stability and biocompatibility. It is reported that flavonoids and phenolic chemicals found in the extract are expected to be responsible for the conversion of metal ions to metal oxide nanoparticles[26] for the preparation of the extract, clean Albizia Amara leaves were boiled in 100 mL double distilled water for 10 min, and filtered using Whatman filter paper. The extract was stored in a refrigerator at 4 °C. For the synthesis of Ni/SrO nanoparticles, 0.1 M $Sr(NO_3)_26H_2O$ and 0.1 M nickel nitrate was mixed in 10:1 into 10 mL of plant extract solution using a magnetic stirrer for 1 hour at 60 °C and the color of the solution turned to a greenish color. Afterward, the solution was centrifuged, washed and dried in a hot air oven at 90 °C and calcined at 450 °C in a muffle furnace to produce SrO and Ni-doped SrO nanoparticles. Finally, the dried sample was collected and crushed into powder for further analysis.

ISSN No. 2321-2705 | DOI: 10.51244/IJRSI |Volume XIII Issue V May 2026

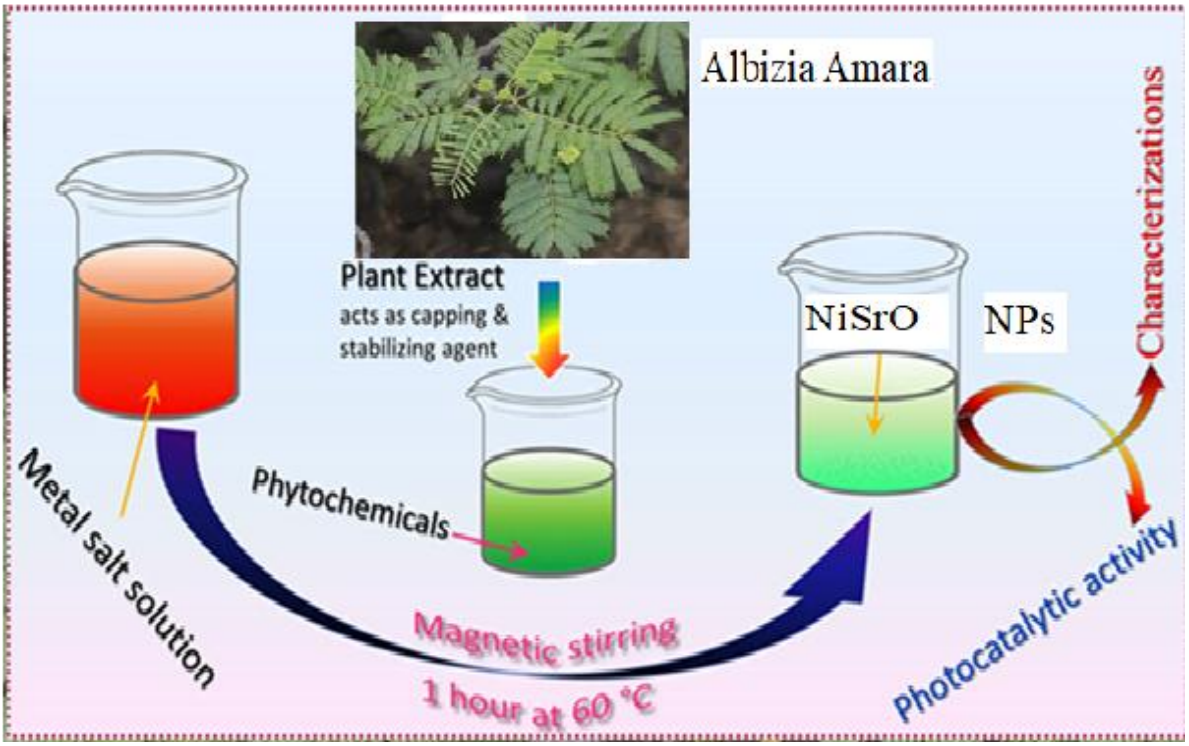

Characterization

The LABINDIA UV 3092 Spectro-photometer was utilized to record the highest absorption and optimize generated NPs. The researchers used a single beam optical detector with a bandwidth of 1nm and a spectrum was recorded of 190 to 1100 nm. It used wavelengths ranging from 200 nm to 800 nm.

FTIR spectroscopy of nickel-doped strontium oxide (Ni-SrO) typically identifies metal-oxygen bonding, with Ni-O stretching peaks located around 402–581 cm^{-1} and Sr-O vibrations appearing in the lower frequency region, often near 854–855 cm^{-1}. Doping induces small shifts in these peaks, confirming structural changes.

Strontium Oxide NPs' crystal-like structure will be investigated. Drops of Strontium Oxide NPs produced from strontium nitrate were placed on the glass for X-ray diffraction at Diffractometer apparatus was maintained running at a current of 20 milliamperes and a voltage of 40 kilovolts, with Cu K radiation being used in addition.

Scanning Electron Microscopy (SEM) and Energy-Dispersive X-ray (EDX) spectroscopy are essential tools for characterizing the structural and elemental properties of Nickel-doped Strontium Oxide (SrO:Ni) materials, often synthesized for applications in photocatalysis, sensors, or magnetic devices. Studies show that Ni doping alters the morphology, crystallite size, and band gap of nanoparticles.

The photocatalytic activity of Albizia Amara facilitated Ni-SrO nanoparticles was tested against naphthol blue black (NBB) dye under visible light irradiation. For this purpose, the Ni-SrO catalyst was added to a polluted water sample (containing 10 ppm NBB molecules) and placed under dark conditions for 20 min to reach the adsorption–desorption equilibrium. After that, the dark-conditioned samples were taken out and kept directly under a visible light source (xenon lamp; power = 150 W & l = 400 nm). The solution was irradiated for 80 min, and during this process at regular time intervals of 20 min, a test sample was collected from the solution. The collected samples were centrifuged to remove the Ni-SrO catalyst from the solution. The degradation efficiency was calculated from the UV-Vis spectra using eqn (1):

$$\text{Dye degradation efficiency } (\%) = \frac{C_0 - C_t}{C_0} \times 100 \qquad (1)$$

Where C_0 is the initial concentration of the NBB dye solution without irradiation with light and C_t is the concentration of the dye solution at different time intervals upon irradiation with visible light. To ensure the

ISSN No. 2321-2705 | DOI: 10.51244/IJRSI |Volume XIII Issue V May 2026

accuracy of degradation efficiency, the experiment was repeated three times under similar conditions.

RESULTS AND DISCUSSION

The morphological, visual features, and structural, of improved Ni\SrO were investigated utilizing a variety of approaches in this study. The photocatalytic degradation of produced photocatalysts was then evaluated using the degradation of NBB dye under light.

UV-Visible spectroscopy

UV-visible is a quick, cheap, and easy characterization approach extensively employed in Nano Materials studies. Because the optical characteristics of certain metal nanomaterials are thoughtful to size, shape, concentration, aggregation state, and refractive index closer to the surface, UV-visible spectroscopy is a helpful method for characterizing them. The UV-visible spectra of SrO and Ni-doped SrO Nps were measured from 200 to 800 nm, and the UV-Vis spectra of SrO and Ni/SrO nanoparticles were measured. Figure 3.1 displays a broad wide excitonic absorption band at 295 nm with a band gap of roughly 4.1 eV. The absorption edges are gradually expanded to longer wavelength regions after Ni doping to reduce band gaps. Interestingly Ni/SrO nano size crystals show absorption boundaries at 309,312 and 317nm, respectivel. The Tauc plot was used to calculate the optical energy band gaps. The pure and doped band gaps Nanocrystals of Ni-doped SrO are 4.2 and 3.91 eV, respectively, based on absorption spectra as shown in (Figure 1). Based on these results, it is obvious that as the amount of Ni increases, the band gap energies decrease slowly, which has a significant impact on the photocatalytic activity of SrO nanoparticles[15,.]

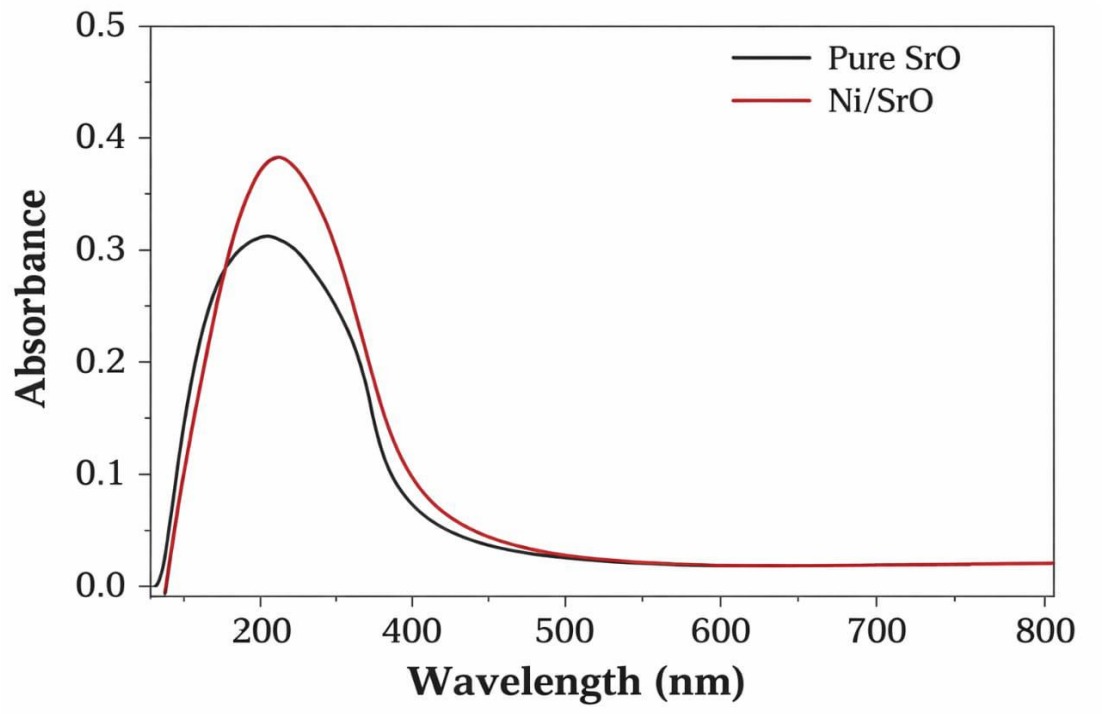

Figure 1. UV-visible spectra of strontium oxide and Ni-doped strontium oxide nanoparticle

Fourier transform infrared spectroscopy (FTIR)

Spectrum FTIR method is utilized to classify various functional groups in materials. Because the strength of the FTIR peak is a significant indication of the type of constituents present, it is an excellent instrument for qualitative research[30]. Figure 3.3 depicts the FTIR spectrum recorded between 4000 and 400 cm-1. The maximum of Ni–O–H bending vibrations and Ni–O stretching may be seen at approximately 405 cm-1 and 582 cm-1, respectively[31]. The indication at 854.84 cm-1 in the FTIR spectra of strontium oxide nanoparticles is caused by Sr–O stretching[5]. The H-O-H bending has significant peaks at 1435.77 cm-1 and 1770.29 cm- 1, as illustrated in (Figure 2). The peak at 3000-3600 cm-1 represents the –OH group and interstitial water molecules.

ISSN No. 2321-2705 | DOI: 10.51244/IJRSI |Volume XIII Issue V May 2026

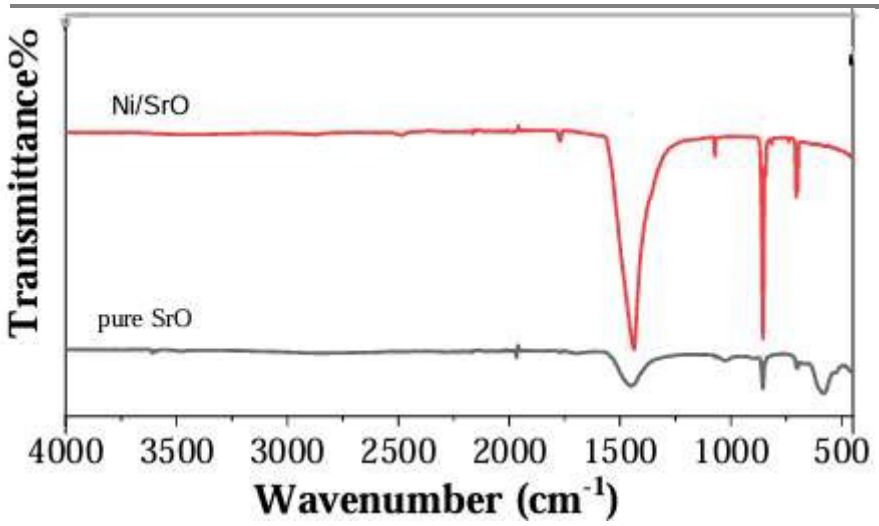

Figure 2: FTIR spectrum of pure and Ni-doped SrO

X-ray diffraction (XRD)

XRD is an operative nondestructive method for characterizing nanocrystals[32]. It's utilized to calculate structures, phases, preferred crystalline structure (texture), and other structural information like mean particle size, strain, crystalline nature, and crystal deficiencies.

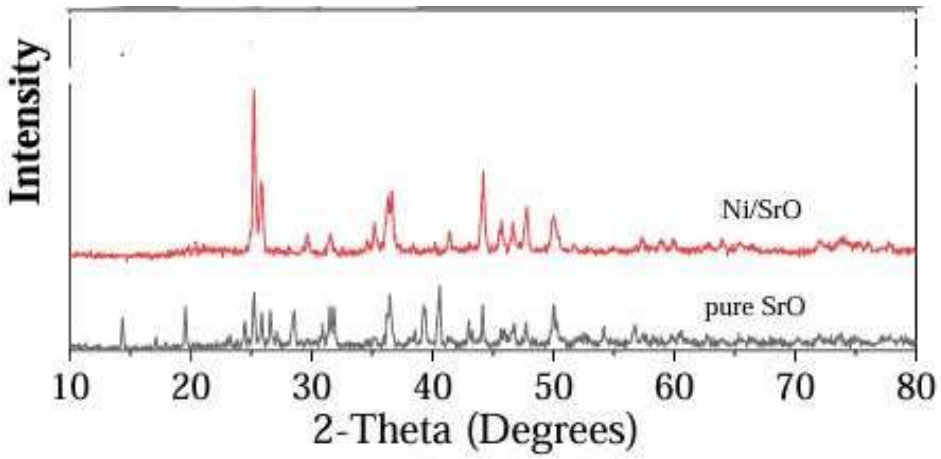

Figure 3: XRD Spectra of pure and Ni-doped SrO

Figure 3 depicts the XRD results from our sample. Pure SrO has nine distinct and strong XRD peaks at 2 = 14, 19, 24, 25, 28, 31, 35, 36, and 39°, which correspond to crystal planes (101), (112), (200), (202), (114), (213), (222), (310), and (312), respectively[33]. These XRD peaks are very narrow and crispy, specifying that the samples are very highly crystalline materials (indicates the decent crystallinity of the Strontium oxide samples). Interestingly, the inclusion of Ni as a dopant promotes the formation of (202) and (310) crystal planes, while the strength of the XRD peak at 19° has been greatly enhanced[34]. The average crystallite diameters of pure, and doped Ni/SrO nanoparticles were determined in this study to be 45 nm and 36nm, respectively. All samples are roughly the same size, with no discernible peak change in the XRD pattern. Furthermore, when the quantity of nickel dopant increases, so does the XRD peak intensity as clearly shown in (Figure 3.2). Ni ions enter the strontium lattice. If no extra impurity peaks appear, it indicates successful doping and good phase purity.

Scanning electronic microscopy (SEM)

SEM pictures of Ni-doped SrO nanoparticles at diverse magnifications are shown in Figure 4 (a, b). The SEM images reveal that the nanostrips with Ni dopant had a smooth surface. Particles of various sizes are observed with cubical and cylindrical morphologies. Furthermore, when the Ni dopant increases, a significant reduction in agglomeration is seen.

ISSN No. 2321-2705 | DOI: 10.51244/IJRSI |Volume XIII Issue V May 2026

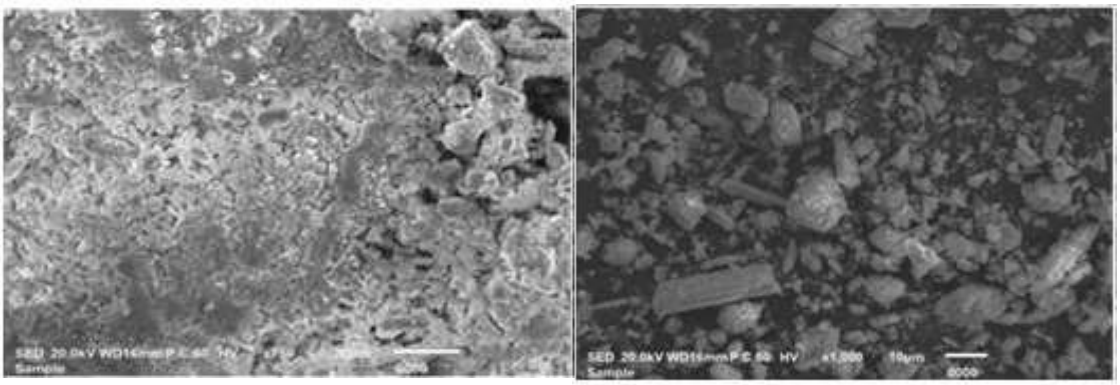

Figure 4: SEM images of pure and Ni-doped strontium oxide.

Energy dispersive X-Ray (EDX)

The fundamental compositions of samples are as small as limited cubic micrometers and are commonly identified and analyzed using the EDX technique. The EDX data and elemental composition of the Ni/SrO sample are shown in (Figure 5). All the essential elements are present in the samples indicating the high purity of the samples. Also, strontium and oxygen are present in a high amount while the doped Ni is about 1.34% in the sample Ni/SrO.

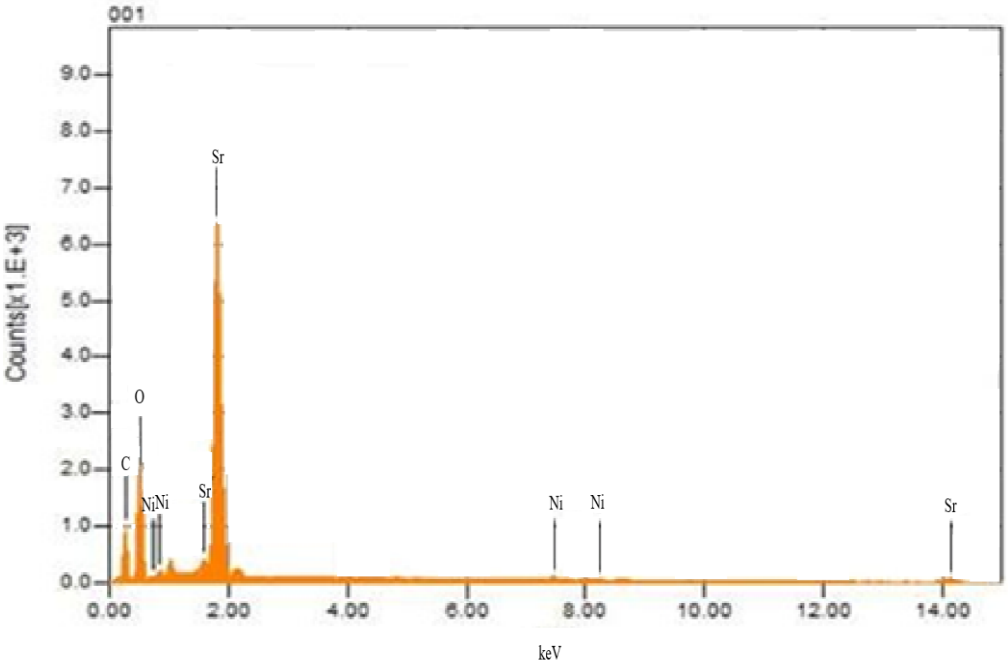

Figure 5: EDX curve of Ni-doped SrO

Photodegradation of Naphthol Blue Black (NBB) dye with UV- light: Primary analysis

The photodegradation of Naphthol Blue Black (NBB) dye in aqueous medium in the presence of catalyst (Ni-SrO) and the atmospheric air were studied using multi lamp photoreactor with mercury UV lamps of wavelength 315 nm. The initial dye concentration $1x10^{-4}$ M and the pH of dye is neutral (pH=7). It was shown to the dark in colour. After the photodegradation colour changes at irradiation times 40 min shown in respectively. The reaction time affords the photodegradation of Naphthol Blue Black (NBB) dye. Thus Ni-SrO exhibited very superior photocatalytic activity when compared to that of SrO and Nil catalyst shown in **Figure. 6.** The NBB dye is resistant to photolysis with Ni-SrO nanocomposite material in the dark in dye (1 X 10^{-4}) concentration was observed NBB dye undergoes % of degradation 0, 31, 75 and 84 % that of SrO % of degradation 0, 17, 38 and 59 % under UV- light in 45 min irradiation the reaction time was affords the photodegradation of NBB dye on Ni-SrO nanocomposite material very superior photocatalytic activity[35-38].

ISSN No. 2321-2705 | DOI: 10.51244/IJRSI |Volume XIII Issue V May 2026

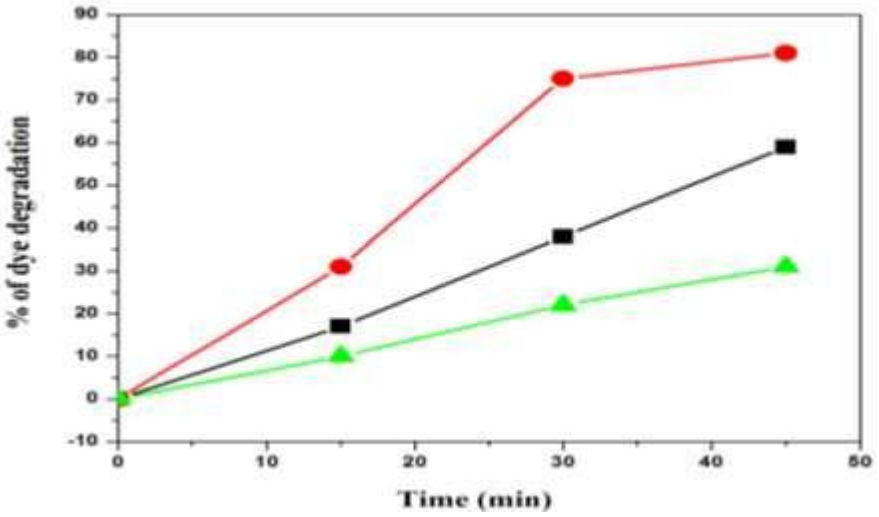

Figure 6: Photodegradation of NBB dye with Nil, SrO and Ni-SrO catalyst

Effect of pH

The pH analysis in photodegradation of NBB dye compared to fast dye was investigated in the pH range 3, 7, 9 and 11 the results are reported. It is observed that the degradation increases with an increase in pH up to 7 and then decreases. After 45 min of irradiation, the percentages of NBB dye degradation are Ni-SrO [18, 46, 84, 28 & 20] that of SrO [12, 29, 59,

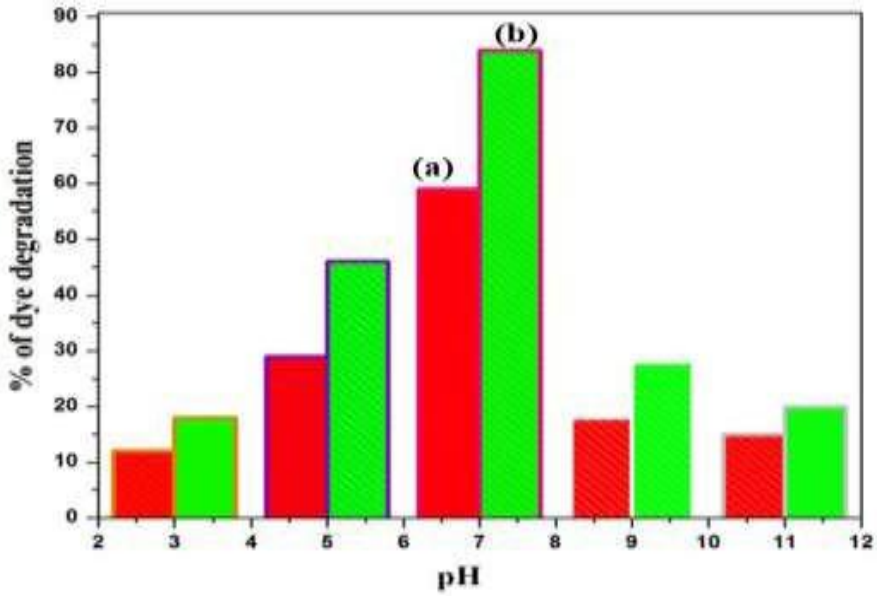

Figure.7. pH study of SrO and Ni-SrO

18 & 15] this pH 3, 5, 7, 9, and 11, respectively. The optimum pH is found to be 7 for NBB dye degradation. Low removal efficiency at the acidic pH range may be due to the dissolution of Ni-SrO nanocomposite material it shows in **Figure.7.**

Effect of catalyst loading

Experiments performed with different amounts of Ni-SrO nanocomposite material showed that the photodegradation efficiency increased with an increase in amount up to 0.08 g/ 50 ml and then then slightly decrease as observed in **Figure. 8.** a and b Catalyst loadings of 0.05, 0.08 and 0.1 g/50ml, respectively. The results show that the of 0.03,0.05, 0.08 and 0.1 g catalyst loading by Ni-SrO nanocomposite material in the dark in dye ($1 X 10^{-4}$) concentration was observed NBB dye undergoes % of degradation 48, 84 and 36 % that of SrO 35, 59 & 25%

ISSN No. 2321-2705 | DOI: 10.51244/IJRSI |Volume XIII Issue V May 2026

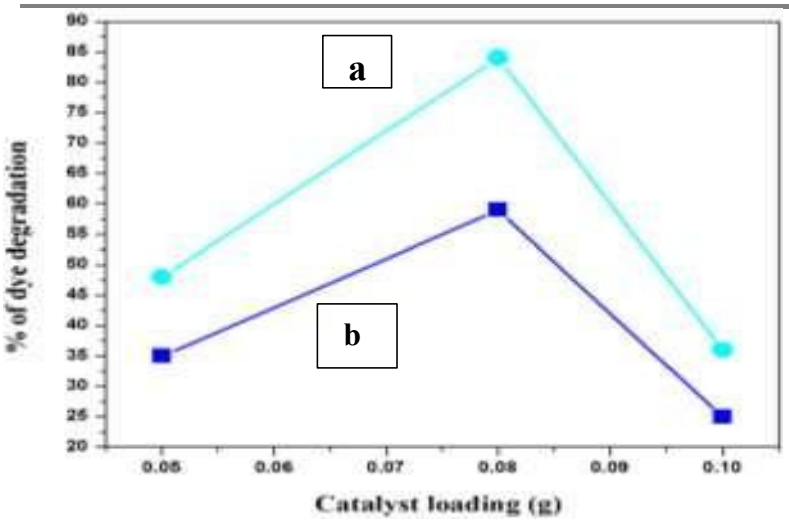

Figure. 8. Effect of catalyst loading

Effect of different concentrations of NBB dye

The effect of dye concentration on the photodegradation of Naphthol Blue Black NBB dye on Ni-SrO nanocomposite material be investigation of $2X10^{-4}$ and $3x10^{-4}$ concentration decrease photodegradation that of $1x10^{-4}$ concentration shows in **Figure. 9.** [39-45].

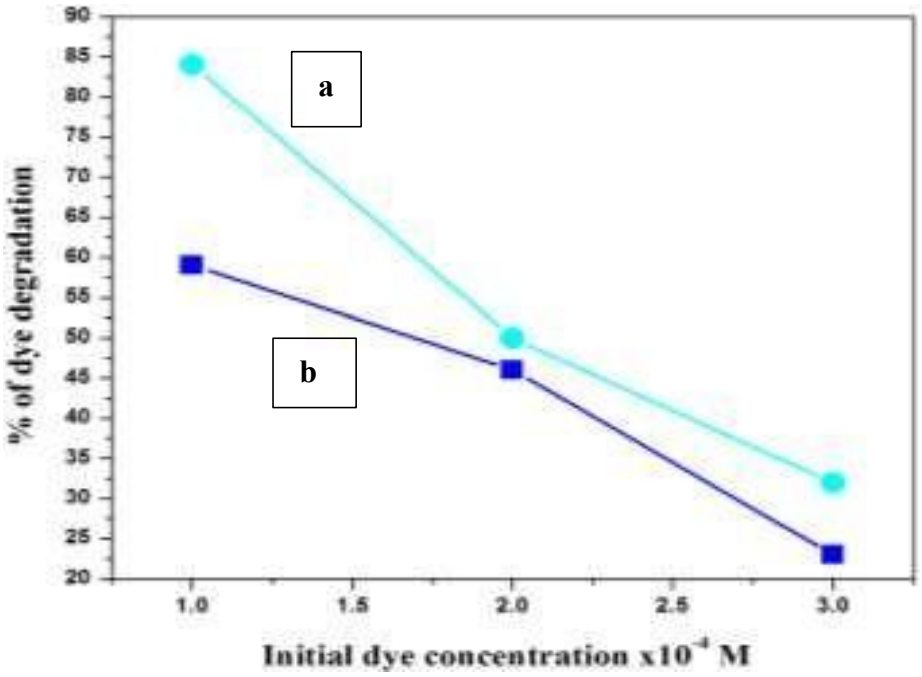

Figure. 9. Effect of concentrations of NBB dye

Stability and Reusability

The reusability of SrO and Ni-SrO nanocomposite material the photocatalytic degradation properties of the photocatalyst was investigated by repeating NBB photocatalytic degradation experiments four times. After each cycle, the photocatalysts were washed thoroughly with water, and a fresh solution of NBB was made before each photocatalytic run in the photoreactor. Under UV- light and the results are shown in **Figure.10.** The complete degradation occurred in the SrO and Ni-SrO nanocomposite material 1st, 2nd 3rd and 4th cycles obtained 100, 90, 85 & 85 % and 100, 98, 90 & 90 % degradation. The results indicated the prepared catalysts are stable and reusable. Also indicates that the photocatalytic efficiency of Ni-SrO nanocomposite material was decreased slowly with increase the repetition of the cycles. This is due to the loss of catalysts, during the water washing of catalysts, which was not observed in the naked eye.

ISSN No. 2321-2705 | DOI: 10.51244/IJRSI |Volume XIII Issue V May 2026

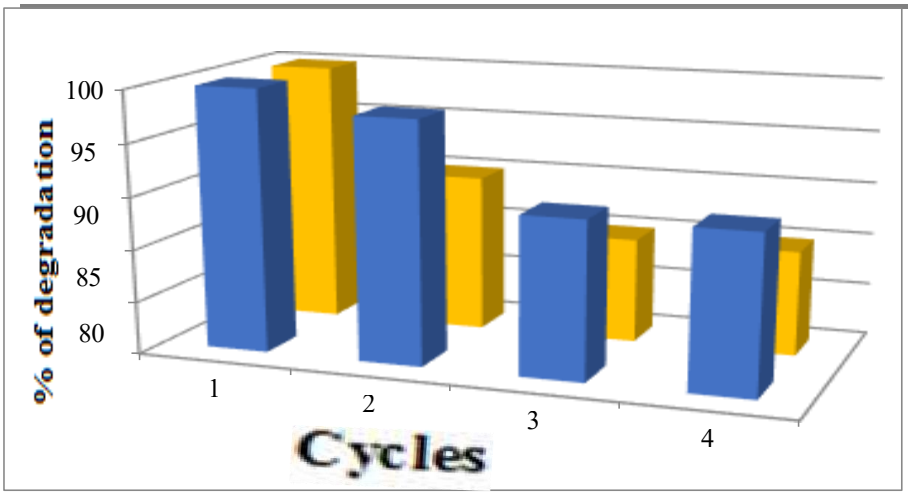

Figure 10: stability and reusability of Ni-Doped SrO nanocomposite

CONCLUSION

Ni-SrO nanomaterial has been synthesized using plant extract as an effective resource for the synthesis of the material. The method is more accessible and environmentally friendly in comparison to other traditional methods. The plant extract has been found to be an efficient capping and stabilizing agent that is responsible for controlling particle size, morphology, structure and other characteristic features of the synthesized material. XRD results confirmed the structure of Ni-SrO nanoparticles, whereas EDX analysis and mapping substantiate the higher amount of Sr, Ni and O element, with weight percentages of 67.2, 20 and 32.8% of the total weight, respectively. The results of FTIR showed the presence of phyto constituents which assist the formation of Ni-SrO NPs. The photocatalytic response of Ni-SrO nanoparticles has been tested against the degradation of NBB dye under visible light irradiation. The photo- degradation efficiency of 87.4% indicate that the Ni-SrO nanoparticles act as an efficient and active photocatalyst. After the 4th cycle of the experiment with the same Ni-SrO photocatalyst, the efficiency is 68.1%, showing its capacity for reuse and potential for commercial use. From this study, we recommend an eco-friendly Albizia amara mediated Ni-SrO photocatalyst prepared via a green synthesis method with enhanced photocatalytic activity under eco-friendly conditions, i.e. UV light irradiation. From the results, it is observed that Ni-SrO can be used to treat cationic dye pollutants dissolved in water.

REFERENCES

1. Madani, S. S., Habibi-Yangjeh, A., Asadzadeh-Khaneghah, S., Chand, H., Krishnan, V., & Zada, A. (2021). Integration of $Bi_4O_5I_2$ nanoparticles with ZnO: impressive visible-light-induced systems for elimination of aqueous contaminants. Journal of the Taiwan Institute of Chemical Engineers, 119, 177-186. https://doi.org/10.1016/j.jtice.2021.01.020.
2. Gupta, S. M., & Tripathi, M. (2012). An overview of commonly used semiconductor nanoparticles in photocatalysis.High Energy Chemistry, 46, 1-9. https://doi.org/10.1134/S0018143912010134.
3. Liu, L., Zhang, X., Yang, L., Ren, L., Wang, D., & Ye, J. (2017). Metal nanoparticles induced photocatalysis. National Science Review, 4(5), 761-780. https://doi.org/10.1093/nsr/nwx019.
4. Zada, A., Humayun, M., Raziq, F., Zhang, X., Qu, Y., Bai, L., Quin, C., Jing, L., & Fu,H. (2016). Exceptional visible-light-driven cocatalyst-free photocatalytic activity of g- C3N4 by well-designed nanocomposites with plasmonic Au and SnO2. https://doi.org/10.1002/aenm.201601190.
5. Ghani, I., Kashif, M., Khattak, O. A., Shah, M., Nawaz, S., Ullah, S., Murad, S., Naz, S., Khan, H. W., Muhammad, S. & Jamal, M. (2023). Hydrothermal synthesis and characterization of Cobalt doped Bismuth oxide NPs for photocatalytic degradation of methyl orange dye. Journal of Xi'an Shiyou University, Natural Science Edition, 19(7), 1195-1217. https://www.xisdxjxsu.asia/viewarticle.php?aid=2506.
6. Yadav, N., Chaudhary, L., Sakhare, P., Dongale, T., Patil, P., Sheikh, A. D. (2018). Impact of collected sunlight on ZnFe2O4 nanoparticles for photocatalytic application. Journal of Colloid and Interface

Science, 527, 289-297. https://doi.org/10.1016/j.jcis.2018.05.051.
7. Kashif, M., Muhammad, S., Ali, A., Ali, K., Khan, S., Zahoor, S., & Hamza, M. J(2023). Bismuth oxide nanoparticle fabrication and characterization for photocatalytic bromophenol blue degradation. Journal of Xi'an Shiyou University, Natural https://www.xisdxjxsu.asia/viewarticle.php?aid=2457.
8. Zada, A., Qu, Y., Ali, S., Sun, N., Lu, H., Yan, R., & Jing, L. (2018). Improved visible- light activities for degrading pollutants on TiO2/g-C3N4 nanocomposites by decorating SPR Au nanoparticles and 2, 4-dichlorophenol decomposition path. https://doi.org/10.1016/j.jhazmat.2017.09.005 Journal of Hazardous Materials, 342, 715-723.
9. Yarahmadi, M., Maleki-Ghaleh, H., Mehr, M. E., Dargahi, Z., Rasouli, F., & Siadati, M. H. (2021). Synthesis and characterization of Sr-doped ZnO nanoparticles for photocatalytic applications. Journal of Alloys and Compounds, 853,157000. https://doi.org/10.1016/j.jallcom.2020.157000.
10. Muhammad, S., Ali, A., Shah, J., Hamza, M., Kashif, M., Khel, B. K. A., & Iqbal, A. (2023). Using Moringa oleifera stem extract for green synthesis, characterization, and anti-inflammatory activity of silver oxide nanoparticles. Natural and Applied Sciences International Journal (NASIJ), 4(1), 80-97. https://doi.org/10.47264/idea.nasij/4.1.6.
11. Ahsan, M., Qasim, S., Shah, A., Nawaz, I., Kashif, M., & Ahmad, W. J. B. J. O. S. (2024). Loading of anticancer drug using Fe3O4@ SiO2. Brazilian Journal of Science, 3(2), 93-101. https://doi.org/10.14295/bjs.v3i2.497.
12. Zada, A., Khan, M., Khan, M. A., Khan, Q., Habibi-Yangjeh, A., Dang, A., & Maqbool, M. J. E. R. (2021). Review on the hazardous applications and photodegradation mechanisms of chlorophenols over different photocatalysts. Environmental Research, 195, 110742. https://doi.org/10.1016/j.envres.2021.110742.
13. Niaz, M., Abrar, H., Ashfaq, S., Khan, N., Awais, M., e Baseerat, N., Jadoon, R., Abrar, A., Kashif, M., & Ullah, K. (2024). Qualitative phytochemical analysis and in vitro antibacterial activity of Punica granatum. Phytopharmacology Research Journal, 3(1), 31-38. https://www.ojs.prjn.org/index.php/prjn/article/view/64.
14. Kashif, M., Ali, M., Naz, S., Amir, J., Murad, S., Atif, M., Khattak, O. A., Ukkah, S., Aleena, S., Khan, N. & Khan, M. Y. (2024a). Formulation development and characterization of quercetin loaded poly caprolactone nanoparticles for tumors. Brazilian Journal of Science, 3(2), 82-92. https://doi.org/10.14295/bjs.v3i2.494.
15. Xu, B., Zada, A., Wang, G., Qu, Y. (2019). Boosting the visible-light photoactivities of BiVO4 nanoplates by Eu doping and coupling CeO x nanoparticles for CO2 reduction and organic oxidation. Sustainable Energy & Fuels, 3(12), 3363-3369. https://doi.org/10.1039/C9SE00409B.
16. Ali, N., Zada, A., Zahid, M., Ismail, A., Rafiq, M., Riaz, A., & Khan, A. J. J. o. t. C. C. S. (2019). Enhanced photodegradation of methylene blue with alkaline and transition- metal ferrite nanophotocatalysts under direct sun light irradiation. Journal of the Chinese Chemical Society, 66(4), 402-408. https://doi.org/10.1002/jccs.201800213.
17. Raziq, F., Aligayev, A., Shen, H., Ali, S., Shah, R., Ali, S., Bakhtiar, S. H., Ali, A., Zarshad, N., Zada, A., Xia, X., Zu, X., Khan, M., Wu, X., & Kong, Q. (2022). Exceptional photocatalytic activities of rGO modified (B, N) Co-doped WO3, coupled with CdSe QDs for one photon Z-scheme system: a joint experimental and dft study. Advanced Science, 9(2), 2102530. https://doi.org/10.1002/advs.202102530.
18. Shah, M., Hameed, A., Kashif, M., Majeed, N., Muhammad, J., Shah, N., Rehan, T., Khan, A., Uddin, J., Khan, A., & Kashtoh, H. (2024). Advances in agar-based composites: a comprehensive review. Carbohydrate Polymers, 346, 122619. https://doi.org/10.1016/j.carbpol.2024.122619.
19. Kashif, M., Jawad, M., Khan, A. A., Sun, H., Ullah, K., Fakayode, O., & Azizi, S. (2024b). Fe/Ti-codoped strontium oxide nanoparticles for enhanced photocatalytic degradation of methyl orange. Journal of Applied Research in Water and Wastewater, 11(1), 8-14. https://doi.org/10.22126/arww.2024.10753.1336.
20. Kashif, M., Khan, A. A., Sun, H., Kamal, J., Shah, M. I. A., Hussain, S., Amir, J., Jamal, Y., & Ahmad, T. (2024c). Synthesis and characterization of Fe-doped CuO nanoparticles: Catalytic efficiency in crystal violet dye degradation and exploration of electrical properties. Brazilian Journal of Science, 3(8), 1-18. https://doi.org/10.14295/bjs.v3i8.601.
21. Khan, M., Hayat, A., Mane, S. K. B., Li, T., Shaishta, N., Alei, D., Zhao, T. K., Ullah, A., Zada, A., Rehman, A., & Khan, W. U. (2020). Functionalized nano diamond composites for photocatalytic

hydrogen evolution and effective pollutant degradation. International Journal of Hydrogen Energy, 45(53), 29070-29081. https://doi.org/10.1016/j.ijhydene.2020.07.274.

22. Xiong, X., Zhang, Y., Wang, L., & Tsang, D. C. W. (2022). Chapter 1 - Overview of hazardous waste treatment and stabilization/solidification technology, in Low Carbon Stabilization and Solidification of Hazardous Wastes, Elsevier, 1-14. https://doi.org/10.1016/B978-0-12-824004-5.00031-1.
23. Şaşmaz, S., Gedikli, S., Aytar, P., Güngörmedi, G., Evrim, A. Ç., Ünal, H. A., Kolankaya, N, 2011. Decolorization Potential of Some Reactive Dyes with Crude Laccase and Laccase-Mediated System. Appl Biochem Biotechnol, 163: 346–361. https://doi.org/10.1007/s12010-010-9043-8.
24. I. Nehdi, Characteristics, chemical composition and utilisation of Albizia julibrissin seed oil, Ind. Crops Prod., 2011, 33,30–34.
25. A. A. Gungor, H. Nadaroglu and D. D. Gultekin, Synthesis and Characterization of Nano-Strontium Oxide (SrO) Using Erzincan Cimin Grape (Vitis vinifera, Cimin), Chem. Sci. Int. J., 2019, 1–7.
26. G. Apsana, P. P. George, N. Devanna and R. Yuvasravana, Biomimetic synthesis and antibacterial properties of strontium oxide nanoparticles using Ocimum sanctum leaf extract, Asian J. Pharm. Clin. Res., 2018, 11, 384–389.
27. V. V Makarov, A. J. Love, O. V Sinitsyna, S. S. Makarova, I. V Yaminsky, M. E. Taliansky and N. O. Kalinina, “Green” nanotechnologies: synthesis of metal nanoparticles using plants, Acta Naturae, 2014, 6,35–44.
28. V. Arya, Living Systems: eco-friendly nanofactories, Dig. J. Nanomater. Biostructures, 2010, 5,9.
29. M. Naseer, U. Aslam, B. Khalid and B. Chen, Green route to synthesize Zinc Oxide Nanoparticles using leaf extracts of Cassia fistula and Melia azadarach and their antibacterial potential, Sci. Rep., 2020, 10,1–10.
30. Athar, T. J. M. F. (2013). Synthesis and characterization of strontium oxide nanoparticles via wet process. Materials Focus, 2(6), 450-453. https://www.ingentaconnect.com/contentone/asp/mf/2013/00002/00006/art00004.
31. Budipramana, Y., Ersam, T., & Kurniawan, F. (2014). Synthesis nickel hydroxide by electrolysis at high voltage. ARPN Journal of Engineering and Applied Sciences, 9(11), 2074-2077. http://www.scopus.com/inward/record.url?scp=84911975219&partnerID=8YFLogxK
32. Hall, J. B., Dobrovolskaia, M. A., Patri, A. K., & McNeil, S. E. (2007). Characterization of nanoparticles for therapeutics. Nanomedicine, 2(6), 789-803. https://doi.org/10.2217/17435889.2.6.789.
33. Sakar, M., Balakumar, S., Saravanan, P., & Jaisankar, S. N. (2013). Annealing temperature mediated physical properties of bismuth ferrite (BiFeO3) nanostructures synthesized by a novel wet chemical method. Materials Research Bulletin, 48(8), 2878- 2885. https://doi.org/10.1016/j.materresbull.2013.04.008.
34. Oskam, G. (2006). Metal oxide nanoparticles: synthesis, characterization and application. Journal of Sol-Gel Science and Technology, 37, 161-164. https://doi.org/10.1007/s10971-005-6621-2.
35. K. T. Ghorai and N. Biswas, J. Mater. Res. Technol., 2013, 2, 10–17. https://doi.org/10.1016/j.jmrt.2013.03.002.
36. B. Subash, B. Krishnakumar, V. Pandiyan, M. Swaminathan and M. Shanthi, Sep. Purif. Technol., 2012, 96, 204–213. https://doi.org/10.1016/j.seppur.2012.06.002.
37. B. Krishnakumar, K. Selvam, R. Velmurugan and M. Swaminathan, Desalin. Water Trea, 2010, 24, 132–139. https://doi.org/10.5004/dwt.2010.1466.
38. B. Krishnakumar, B. Subash and M. Swaminathan, Sep. Purif. Technol., 2012, 85, 35-44. https://doi.org/10.1016/j.seppur.2011.09.037.
39. R. Velmurugan, K. Selvam, B. Krishnakumar and M. Swaminathan, Sep. Purif. Technol., 2011, 80, 119–124. https://doi.org/10.1016/j.seppur.2011.04.018.
40. B.Subash, B.Krishnakumar, M.Swaminathan, M.Shanthi, Journal of Molecular CatalysisA:Chemical,2013,366,5463. https://doi.org/10.1016/j.molcata.2012.09.008.
41. V.L. Chandraboss, J. Kamalakkannan, S. Prabha and S. Senthilvelan, RSC Adv., 2015, 5, 25857. https://doi.org/10.1039/C4RA14463E.
42. A. Mohamed Ibraheem, K. Jayamoorthy, J. Kamalakkannan, G. Selvakumar, D. Rajamanickam. Advanced Assembly of Spherical MoO_3-SnO_2 Nanocomposite Material and Its Catalytic Applications.
43. A. Mohamed Ibraheem, K. Jayamoorthy, J. Kamalakkannan, G. Selvakumar, D. Rajamanickam. Enhanced photocatalysis of $VCrO_4$ doped TiO_2 for dye degradation under UV light.

44. C. Palanivel, N.R. Prabhakaran, G. Selvakumar, Morphological expedient flower like nanostructures WO3–TiO2 nanocomposite material and its multi applications.OpenNano(4),2019,100026, https://doi.org/10.1016/j.onano.2018.11.002.
45. G. Selvakumar, C. Palanivel, Effect of MoO3 Doping on ZnO Nanomaterial for the Reduction of NBB dye under UV-light. International Journal of Research and Analytical Reviews, Volume8, Issue4, November2021, pages772-729. https://doi.one/10.1729/journal.28493.